International Journal of River Basin Management
Publication details, including instructions for authors and subscription information:
http://www.tandfonline.com/loi/trbm20

Estimation of dimension and time variation of local scour at short abutment

Reza Mohammadpour [a], Aminuddin AB. Ghani [b] & Hazi Mohammad Azamathulla [c]

[a] River Engineering and Urban Drainage Research Centre (REDAC), Universiti Sains Malaysia, Engineering Campus, Seri Ampangan, 14300 Nibong Tebal, Penang, Malaysia

[b] Professor and Deputy Director, REDAC, Universiti Sains Malaysia, Engineering Campus, Seri Ampangan, 14300 Nibong Tebal, Penang, Malaysia

[c] Associate Professor, REDAC, Universiti Sains Malaysia, Engineering Campus, Seri Ampangan, 14300 Nibong Tebal, Penang, Malaysia

Accepted author version posted online: 01 Feb 2013.Version of record first published: 21 Mar 2013.

To cite this article: Reza Mohammadpour , Aminuddin AB. Ghani & Hazi Mohammad Azamathulla (2013): Estimation of dimension and time variation of local scour at short abutment, International Journal of River Basin Management, 11:1, 121-135

To link to this article: http://dx.doi.org/10.1080/15715124.2013.772522

Intl. J. River Basin Management Vol. 11, No. 1 (March 2013), pp. 121–135

Research paper

Estimation of dimension and time variation of local scour at short abutment

REZA MOHAMMADPOUR, *PhD Student, River Engineering and Urban Drainage Research Centre (REDAC), Universiti Sains Malaysia, Engineering Campus, Seri Ampangan, 14300 Nibong Tebal, Penang, Malaysia. Email: reza564@gmail.com (Author for correspondence)*

AMINUDDIN AB. GHANI, *Professor and Deputy Director, REDAC, Universiti Sains Malaysia, Engineering Campus, Seri Ampangan, 14300 Nibong Tebal, Penang, Malaysia*

HAZI MOHAMMAD AZAMATHULLA, *Associate Professor, REDAC, Universiti Sains Malaysia, Engineering Campus, Seri Ampangan, 14300 Nibong Tebal, Penang, Malaysia*

ABSTRACT

Accurate prediction of the local scour at abutments is an important criterion to design a safe depth for the bridge foundation. In this paper, the dimension and variation of local scour with time at a vertical-wall abutment were investigated experimentally under clear-water conditions. The multiple linear regression (MLR), gene expression programming (GEP) and artificial neural networks (ANNs), feed forward back propagation and radial basis function were used to predict the time variation of scour depth at a short abutment. Results indicated that the dimension of the scour hole in the *x*-direction ranged from 3L to 5L upstream and downstream of the abutment, respectively, and also 4L in the *y*-direction. Statistical analysis showed that, although the ANNs technique produced better results ($R^2 = 0.997$, RMSE = 0.0113 and MAE = 0.0071) in comparison with the GEP ($R^2 = 0.959$, RMSE = 0.068 and MAE = 0.044) and MLR techniques ($R^2 = 0.958$, RMSE = 0.059 and MAE = 0.041), both GEP and MLR are more practical methods. Finally, sensitivity analysis indicated that the local scour was greatly affected by the three studied parameters in the following order, time ratio (t/t_e) > abutment length ratio (L/y) > velocity ratio (U/U_c).

Keywords: Abutment scour; temporal scour; scour hole dimension; gene expression programming; artificial neural networks

1 Introduction

The economical and safe design of bridges depend on accurate forecasting of the local scour around the abutment. Over the recent years, considerable research has been conducted for the reliable prediction of time-varying scour depth (Sturm and Janjua 1994, Lim 1997, Melville and Coleman 2000, Brandimarte et al. 2012). In particular, a number of empirical formulae have been developed to predict the time variation of scour depth around abutments. However, the suggested equations were limited to the experimental condition for a specific data set (Table 1).

Lately, several studies have reported that methods such as artificial neural networks (ANNs) and gene expression programming (GEP) can provide a good solution to complex problems, in hydraulic engineering such as the estimation of local scour. Bateni et al. (2007) have compared dimensional and non-dimensional parameters for the estimation of time-depended scour depth around piers using ANNs. They showed that the prediction of scour depth based on dimensional data yielded a better result than those obtained from dimensionless data. Sarlak and Tigrek (2011) have used ANNs to assess collected data sets of the abutment scour. The study showed the necessity to determine homogeneity of the data set using the neural networks. The sensitivity analysis they conducted showed that the flow mean velocity is the significant parameter, while abutment width is the least effective parameter for determining the equilibrium scour depth. Begum et al. (2011) predicted the maximum scour depth around a bridge abutment using a radial basis function (RBF) network. The suitability and reliability of ANNs was reported for estimation of scour depth at an abutment, they indicated that the abutment length is a significant parameter, whereas the flow depth is least sensitive for scour depth. Toth and Brandimarte (2011) developed ANNs to estimate the scour depth at

Received 15 July 2012. Accepted 18 January 2013.

ISSN 1571-5124 print/ISSN 1814-2060 online
http://dx.doi.org/10.1080/15715124.2013.772522
http://www.tandfonline.com

Table 1 Empirical formulas to predict time-dependent scour depth around abutment

Reference	Equation	U/U_c	L/y	Standard deviation(σ_g)
Yanmaz and Kose (2007)	$\frac{d_s}{L} = 0.25\,F_d^{0.85}\left(\frac{L}{y}\right)^{0.15}\left(\log\left(\frac{t\,d_{50}\sqrt{g\Delta d_{50}}}{L^2}\right)\right)^{0.6}$	0.68∼0.99	1.12∼2.4	∼1.4
Oliveto and Hager (2002)	$\frac{d_s}{y^{1/3}L^{2/3}} = 0.068N\ \sigma_g^{-0.5}\,F_d^{1.5}\ \log\left(\frac{t\sqrt{g\Delta d_{50}}}{y^{1/3}L^{2/3}}\right)$	–	1.25∼6.0	1.0–2.15
Coleman et al. (2003)	$\frac{d_s}{d_{se}} = \exp\left[-0.07\left(\frac{U}{U_c}\right)^{-1}\left\lvert Ln\left(\frac{t}{t_e}\right)\right\rvert^{1.5}\right]$	0.46∼0.99	0.25∼151	–
Ballio and Orsi (2001)	$\frac{d_s}{d_{se}} = 1-\exp\left[-0.028\left(\frac{tU}{(Ly)^{0.5}}\right)^{0.28}\right]$	≈1	0.27∼1.09	1.3
Cardoso and Bettess (1999)	$\frac{d_s}{d_{se}} = 1-\exp\left[-1.025\left(\frac{t}{T^*}\right)^{0.35}\right]$	0.91∼1.08	2∼23.5	1.26

Note: Where T^* = time when $d_s = 0.632d_{se}$, $\Delta = S\text{-}1$ and S = relative density of sediment particles, N = shape number equal to 1.25 for vertical-wall abutment.

piers under both clear-water and live bed conditions. The result showed that ANNs can predict the local scour in both conditions better than the empirical formula. Begum et al. (2012) used ANNs to estimate the equilibrium depth of scour around semicircular abutments. Both RBF and Multi-Layer Perceptron (MLR) ANNs were trained with experimental data. The result indicated that the neural networks can predict the scour depth at abutment with high accuracy.

Bateni and Jeng (2007) employed the adaptive network fuzzy inference system (ANFIS) and two ANNs models, the MLR and RBF, to estimate time-dependent and maximum scour depth around bridge piers. The MLR method produced a better prediction of scour depth than ANFIS, RBF and the previous empirical approaches. Muzzammil (2010) predicted the scour depth at abutments using both ANNs and ANFIS. The comparison of results illustrated that the ANFIS approach performed best among the regression and ANN models. The ANFIS-based approach was used by Muzzammil (2011) to forecast the scour depth at bridge abutments embedded in an armoured bed. The ANFIS's results were compared with a regression method (RM) and neural networks. It was found that although the RBF produced better predictions than the other ANN training algorithms, the ANFIS model was the best among the ANNs and better than the RM.

To predict scour depth around abutments using expression programming (GEP), Azamathulla (2012) indicated that the GEP gives satisfactory results compared with empirical equations and ANNs. Khan et al. (2012) used data field to predict local scour around piers using the GEP. They showed that predictions using the GEP were acceptable and encouraging when compared with regression and ANN models. Azamathulla et al. (2010) utilized genetic programming (GP) to estimate bridge pier scour. After comparing the performance of the GP with ANNs and regression equations, it was recognized that the GP is more effective than other approaches. All aforementioned techniques have already been applied with some success to estimate only the maximum scour depth around bridge or abutments by various researchers, whereas prediction of the temporal scour depth is a main problem during the flood.

This study evaluates the dimension of local scour at short abutment ($L/y < 1$) and predicts the temporal scour depth using GEP. The explicit GEP equation is compared with regression equation, and ANN methods, RBF and feed forward back propagation (FFBP).

2 Physics of scouring

The presence of bridge abutments may cause a huge change in flow patterns. The main case of the scour at abutment is the primary vortex and associated down-flow in front of the abutment. The primary vortex has an elliptical shape with outer and inner core regions. The inner core occupies 17% of the scour hole area and contains up to 78% of the total circulation in the flow. In vicinity of the abutment, the maximum down-flow component and velocity are 0.75 and 1.35 times the approach flow velocity, respectively (Kwan and Melville 1994). The wake vortices are created in downstream of the abutment due to separation of flow around the abutment.

The scour hole at an abutment develops due to complex vortices; the vortices develop the scour hole in three parts, in front of, to the side of and downstream of the abutment (Dey and Barbhuiya 2005). Due to the complexity in vortices around the abutment, it is difficult to estimate the time-varying scour depth by direct modelling of the vortices. Therefore, empirical equations have typically been developed based on representative parameters from the laboratory experiments. The time, abutment length, flow depth, flow velocity, distribution of the sediment, abutment shape, abutment skew angle, geometry of channel and flow properties have all been considered as representative parameters for determining abutment scour in river or channels. Figure 1 shows a schematic view of the abutment and pier scour.

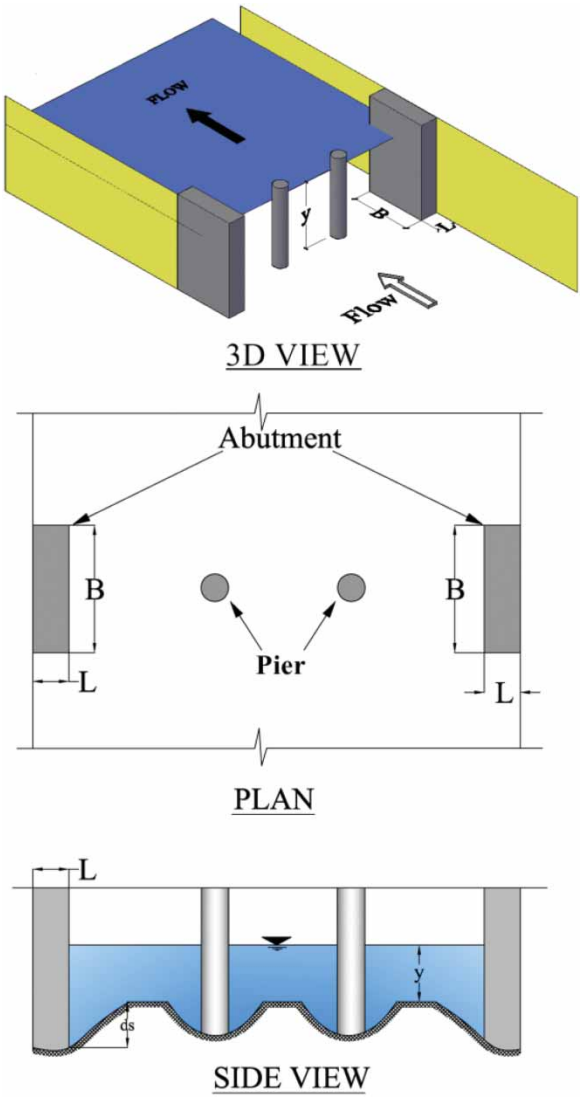

Figure 1 Local scour around abutment and pier.

3 Dimensional analysis

The abutment scour is expressed by the independent variables and parameters as (Melville 1992):

$$d_s = f(t, L, y, U, g, \rho, \nu, d_{50}, \sigma_g, \rho_s, K_\theta, K_s, K_G), \quad (1)$$

where t is the time; L is the abutment length; y is the approach flow depth; U is the mean flow velocity; g is the acceleration due to gravity; ρ and ν are the fluid density and kinematic viscosity, respectively; d_{50} is the median size of the bed material; σ_g is the geometric standard deviation of the sediment; ρ_s is the sediment density; K_θ and K_s are coefficients describing the alignment and the shape of the abutment and K_G is a coefficient describing the geometry of the channel cross-section. A functional relationship can be developed based on the equilibrium time (t_e) and maximum scour depth (d_{se}) using Buckingum's-π theorem derived as (Cardoso and Bettess 1999)

$$\frac{d_s}{d_{se}} = f\left(\frac{t}{t_e}, \frac{L}{y}, \frac{d_{50}}{L}, F_d, Re, \sigma_g, K_\theta, K_s, K_G\right), \quad (2)$$

where $F_d = U/\sqrt{\Delta g d_{50}}$ is the sediment Froude number and $\Delta = (\rho_s - \rho)/\rho$; $Re = UL/\nu$ is the abutment Reynolds number. Assuming a vertical-wall abutment and right angles from the channel side wall are used, $K_s = 1$ and $K_\theta = 1$. For a wide rectangular channel and uniform flow, the scour is not affected by K_G (Melville 1992). Then Eq. 2 can be rewritten as

$$\frac{d_s}{d_{se}} = f\left(\frac{t}{t_e}, \frac{L}{y}, \frac{d_{50}}{L}, F_d, Re, \sigma_g\right). \quad (3)$$

According to Melville and Coleman (2000), the effect of d_{50}/L is negligible if $L/d_{50} > 50$, which reflects most real abutments, and the influence of the Reynolds number is negligible under a fully turbulent flow over a rough bed (Oliveto and Hager 2002). The flow intensity, $I = U/U_c$, can be replace by F_d, defined as the ratio of the mean approach flow velocity to sediment critical velocity (Simarro et al. 2007). For a uniform sediment, the effect of standard deviation is negligible, hence Eq. 3 can be replaced by

$$\frac{d_s}{d_{se}} = f\left(\frac{t}{t_e}, \frac{L}{y}, \frac{U}{U_c}\right). \quad (4)$$

Equation 4 can be used to estimate the time-dependent scour depth for vertical-wall abutments and perpendicular abutments (without any angle to flow) in a wide rectangular channel with uniform flow and sediment.

Table 1 shows the list of equations applied to predict the time variation of scour depth at short abutments proposed by Yanmaz and Kose (2007), Oliveto and Hager (2002), Ballio and Orsi (2001), Cardoso and Bettess (1999) and Coleman et al. (2003) with limitation on U/U_c, L/y and size of the sediment.

4 Experimental set-up

The experiments were carried out in a 6.0 m long, 0.6 m wide and 0.6 m deep laboratory flume at REDAC, equipped with a 25 cm deep sediment recess (Figure 2). The test section was chosen in a way that a uniform flow was established. To reduce the flow turbulence several floatable screens were placed at the entrance of the flume. The flow depth was adjusted to the desired level using a controlling gate at the end of the channel. The flow depth was selected between 97 and 110 mm, such that there were no significant effects of flow depth on the scour hole ($L/y < 1$). The water discharge was controlled by an inlet valve and measured by a triangle weir at the outlet of the flume. For all the experiments, uniform sand with $\sigma_g = 1.14$ and $d_{50} = 0.60$ mm was selected. As shown in Table 2, three different lengths, 4.0, 5.5 and 7.0 cm, were chosen for Test A-1, A-2 and A-3, respectively, and a ratio of length to width (L/B) of 0.5 was selected for each abutment ($L/y \leq 1$).

A long-term experiment was conducted for each abutment until the rate of growth of the scour hole reached close to the equilibrium scour depth. Coleman et al. (2003) defined the time to achieve equilibrium scour as the time that in a period of 24 h the rate of the scour reduces to 5% or smaller of the

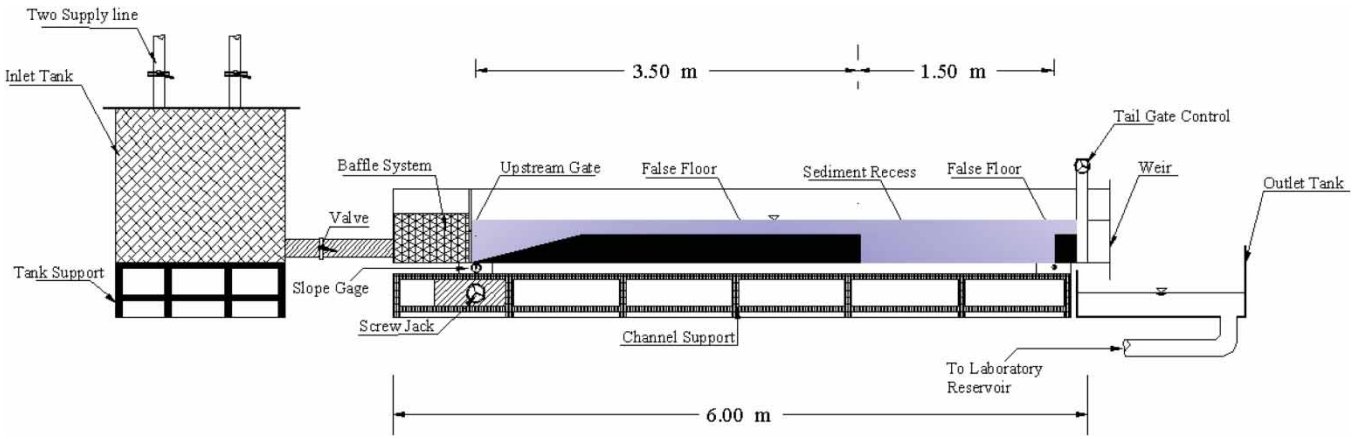

Figure 2 Longitudinal flume section.

Table 2 Summary of experimental results for the present study

Present study	Q (l/s)	U/U_c	Time (min)	d_{50} (mm)	σ_g	L (cm)	B (cm)	y (cm)	L/B	L/y	ds (cm)
A-1	18.00	0.96	3052	0.60	1.14	4.00	8.00	11.10	0.50	0.36	6.70
A-2	18.60	0.98	4004	0.60	1.14	5.50	11.00	11.00	0.50	0.50	9.50
A-3	16.00	0.95	5080	0.60	1.14	7.00	14.00	9.70	0.50	0.72	11.80

flow depth or the abutment length (pier diameter). To measure the depth of the scour, a camera was installed at the upstream end of the abutments where the deepest point usually occurred. Pictures were taken at every 4 min to evaluate the change in scour depth with respect to time. To maintain clear-water conditions, the flow velocity was set close to the critical velocity for the sediment ($U/U_c \approx 1$), where Uc was estimated using the Shields diagram and expressions proposed by Melville and Coleman (2000). The value of Uc was verified and the topography of the scour hole after each run was measured using a point gauge with an accuracy of ± 1 mm.

5 Experimental results

5.1 *Variation of scour depth*

The local scour began to develop at the upstream nose of the abutment and to opposite side of the flume wall. This is due to the primary vortices which sink into the scour hole (Kwan and Melville 1994). Figure 3 shows the local scour hole around the abutment for Test A-3 after 5 and 30 min. In the initial stage, the primary vortices pick up the sediments from upstream of the abutment and the process is continued on the downstream side. The deepest point in this initial test occurs at the nose of the abutment (Figure 3). The scour hole in front of the abutment was observed to enlarge by collapse of the sediment in the scour hole and sediments were then picked up by the primary vortex and deposited around the abutment. Generally, as the depth of the sediment deposition increased, the shear stress increases, and the sediment is carried out by the flow and vortices to the downstream of the abutment. Similar trends were observed for time-varying scour around the abutment for Test A-1 and A-2.

A logarithmic trend was observed around the abutment where the scour depth increased rapidly during the first hours, after this the rate of scour gradually decreased (Figure 4). This figure indicates a comparison between the experimental data obtained during this experiment and the data collected by Yanmaz and Kose (2007), Dey and Barbuhuiya (2005), Ballio and Orsi (2001) and Cardoso and Bettess (1999). The axes on Figure 4 were normilized by the equilibrium time (t_e) and equilibrium scour depth (d_{se}). A good agreement is observed between the present study and the data reported in the literature. The result indicated that maximum scouring occurred during the initial stage of the experiment. Approximately 80–90% of the maximum scour depth occurred during the initial 20–40% of the equilibrium time.

5.2 *Scour hole development*

Figure 5 illustrates a typical scour hole profile around an abutment for Test A-3. The maximum scour depth is usually located in front of the upper corner of the abutment. Figure 6 shows different longitudinal profiles in terms of Y/L around the abutment for Test A-3. The dimensions are normalized using abutment length (L) in both axes where the abutment was located at $X = 0.00$ cm with $L = 7$ cm and $B = 14$ cm. Both upstream and downstream slope of the abutment decreases with increasing Y/L. Also, Figure 7 shows the longitudinal section through the scour hole for all three abutments at different locations: $Y/L = 1$, $Y/L = 1.43$, $Y/L = 2.14$, $Y/L = 3.57$ and $Y/L = 4.00$. The upstream slope was found to be 30–60% greater than the downstream slope. The scour depth and scour hole slope decreased with increasing Y/L and reached zero at $Y/L \geq 4.0$. Therefore, extension of the scour hole in the Y-direction is limited to $4L$. By contrast,

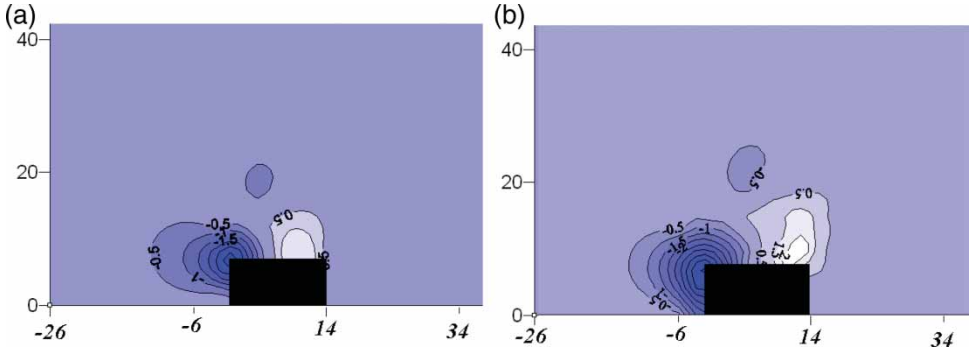

Figure 3 Development of scour hole around abutments in Test A-3 (a) after 5 min and (b) after 30 min.

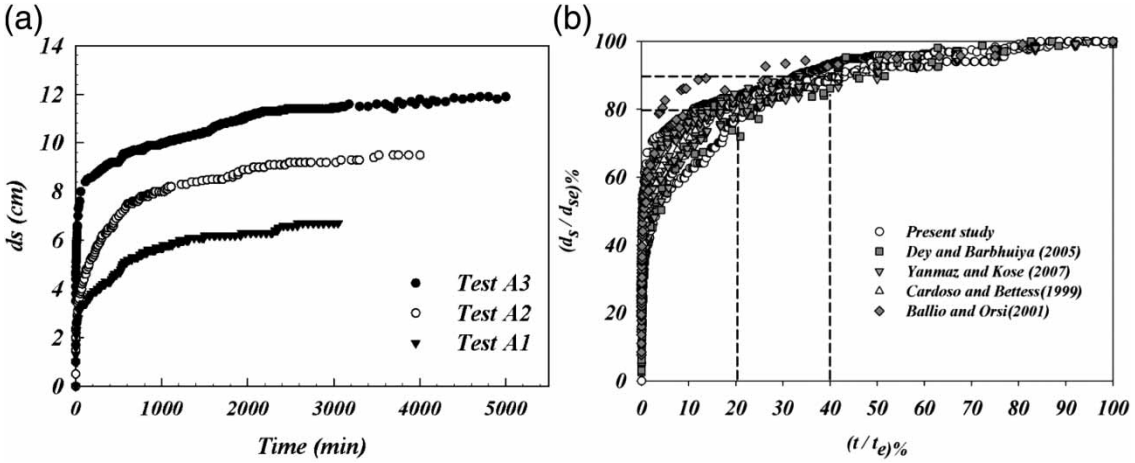

Figure 4 Time variation of scour depth at abutments (a) present study and (b) comparison with collected data.

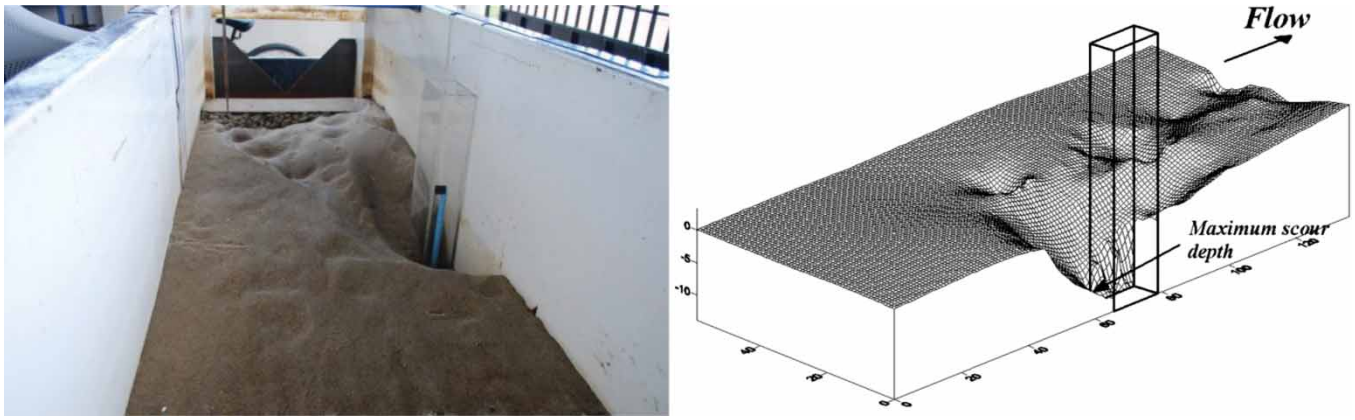

Figure 5 Observed scouring around abutment Test A-3.

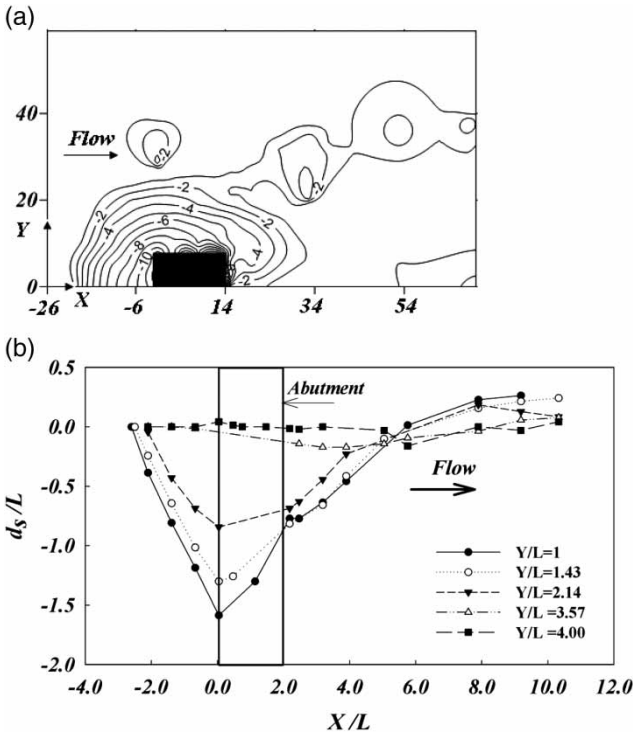

Figure 6 Scour hole around abutment in Test A-3 (a) topography and (b) longitudinal profile.

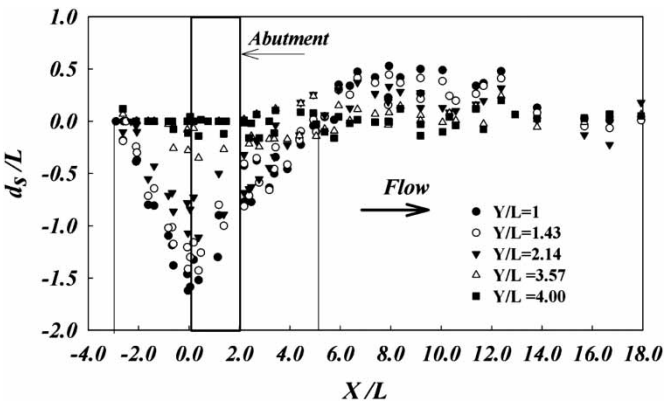

Figure 7 Scour hole around abutments in Test A-1, A-2 and A-3 in different longitudinal sections.

the equilibrium scour hole extended between $X/L = 3$ and $X/L = 5$ upstream and downstream of the abutment in the x-direction. At $X/L > 5$, the sediment started to deposit, and it continued to do so until $X/L = 16$ downstream of the abutment. The maximum depth of the sediment deposition was founded at $X/L = 9$, near to channel side. The depth of the sediment deposition decreased with increasing Y/L and reached zero at $Y/L = 4.0$.

6 ANN methods

ANN is a data-processing tool which attempts to represent the low-level intelligence of the human brain. The smallest part of the neural network is termed a neuron and these artificial neurons are arranged in the structure like a network. In this study, two models of neural networks, FFBP and RBF are presented.

6.1 *FFBP neural network*

Figure 8 shows topography of a FFBP neural network which consists of a set of neurons in three inputs, hidden and output layer. The number of hidden layers and nodes in each layer has been detected by trial and error. First, a set of input data (x_1, x_2, … x_R) is fed to the input layer, and the output of each neuron can be determined from the relation (Bateni et al. 2007):

$$n = \sum w_{ij}x_i + b_i, \tag{5}$$

where n is the neuron output, w_{ij} is the weight of the connection between the jth neuron in the present layer and the ith neuron in the previous layer, x_i is the neuron value in the previous layer and b_i is the bias. To generate the result, the output of each neuron passes through a transfer function, which is generally a sigmoid function (Bateni et al. 2007) given by

$$y_i = \frac{1}{1 + e^{-C\left(\sum w_{ij}x_i + b_i\right)}}, \quad C > 0. \tag{6}$$

The network error is determined by comparing between the target value and obtained result, and the weight between neurons is corrected using the back propagation algorithm.

6.2 *RBF neural network*

An RBF network is a general regression tool for function approximation. Figure 9 indicates the configuration of an RBF network with R neurons in the input layer, where the RBF

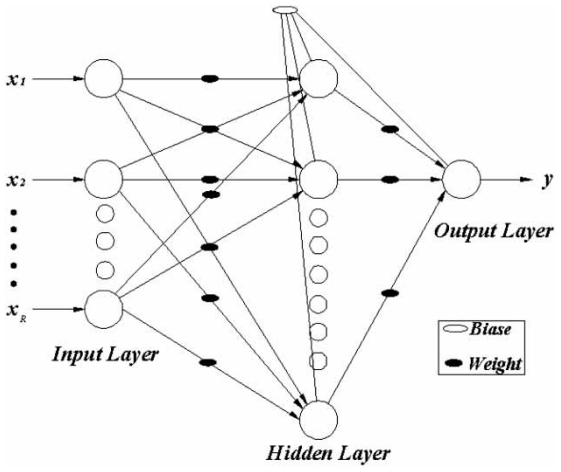

Figure 8 Architecture of the feed forward neural network.

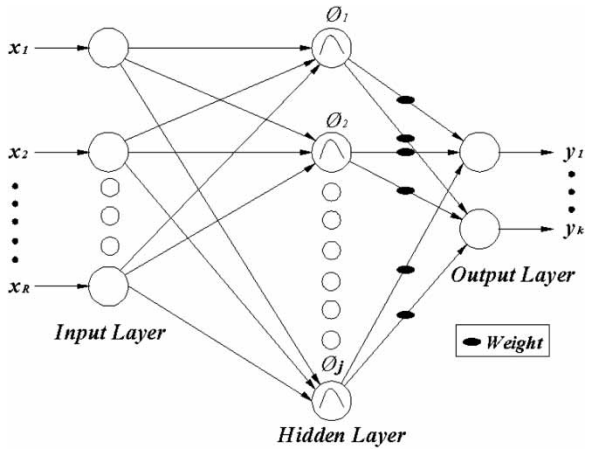

Figure 9 Architecture of the radial basis function network.

output from the jth hidden node is defined as φ_j. In this study, the Softmax transfer function (Bateni and Jeng 2007) is used to estimate the φ value at each node

$$\varphi_j(x) = \frac{\exp\left(-\left(\left\|x - \mu_j\right\|^2 / 2\sigma_j^2\right)\right)}{\sum \exp\left(-\left(\left\|x - \mu_j\right\|^2 / 2\sigma_j^2\right)\right)}, \tag{7}$$

where x is the input data set, μ_j is centre of the RBF for the jth hidden node, σ_j is the radius of the RBF for the jth hidden node and $\left\|x - \mu_j\right\|^2$ is the Euclidean norm. The output of the RBF is linear interconnected to hidden nodes, which can be expressed by the following equation (Bateni and Jeng 2007):

$$y_k = \sum w_{kj}\varphi_j(x), \tag{8}$$

where y_k is the kth component of the output layer, $w_{k\,j}$ is the weight between the jth hidden node and kth node of the output layer. In this study, both input and output data were normalized for training and testing, this normalization is performed within the range of 0.1–0.9 (Begum et al. 2012):

$$X_n = \frac{0.8(X - X_{\min})}{(X_{\max} - X_{\min})} + 0.1, \tag{9}$$

where X_n is the normalized value of X. The $X_{\min}$ and $X_{\max}$ are the minimum and maximum value of each variable of the original data, respectively.

To validate the results, three common error measures, namely the coefficient of correlation (R^2), root mean square error (RMSE) and mean absolute error (MAE) were used. The expressions for these measures are given by (Bateni and Jeng 2007)

$$R^2 = 1 - \frac{\sum_{i=1}^{p}(O_i - t_i)^2}{\sum_{i=1}^{p}(O_i - \overline{O_i})^2}, \tag{10}$$

$$\mathrm{RMSE} = \sqrt{\frac{\sum_{i=1}^{p}(O_i - t_i)^2}{n}}, \tag{11}$$

$$\mathrm{MAE} = \frac{1}{n}\sum_{i=1}^{p}|O_i - t_i|, \tag{12}$$

where O_i is an observed value, t_i is the predicted value and $\overline{O}_i$ is an average of the observed values and n is the number of samples.

7 Verification of the collected data

Extensive library data sets were used to predict the time-dependence of scour at short abutments ($L/y \leq 1$) from this study and earlier studies by Dey and Barbhuiya (2005) and Ballio and Orsi (2001). To avoid the effect of the sediment size on the scour depth, a data set of uniform sediment was selected ($\sigma_g < 1.35$). Table 3 presents a summary of 995 collected data for different parameters.

It can be found that 72 data from the Ballio and Orsis's study showed a ratio of L/y larger than 1 ($L/y = 1.08$). These abutments can be considered as short abutments, in comparison with long abutments ($L/y > 25$). Table 3 shows that all collected data were run under clear-water conditions ($U/U_c < 1$).

To evaluate the reliability of the data sets, tests were undertaken using a simple FFBP network with three dimensionless parameters as per Eq. 4 with t/t_e, L/y and U/U_c as the inputs, three neurons in the hidden layer and one neuron in the output layer. Approximately 80% of the data was randomly selected for training and the remaining 20% was used for testing the model. Then each group of data sets were removed from all the data one by one and the same network was run for each test (Table 4). The process was stopped as the number of iterations exceeded a prescribed maximum of 4000, or a suitable level of error was achieved. From Table 4, it can be noted that the values of R^2 and RMSE for all testing data were very close to each other, although the accuracy was slightly increased by removing Ballio and Orsi's data from the data set ($R^2 = 0.988$ and RMSE $= 0.0187$). This finding showed that the variation of statistical values is minimal by excluding a group of data set. In Table 4, since difference between statistical values is ignorable for a simple network with three neurons in the hidden layer; consequently, the collected data including 995 different data sets can be gathered in a group data set for neural networks (Sarlak and Tigrek 2011).

8 Development of ANNs models

The 995 data sets were divided randomly into training and testing subsets, 80% (800 member data set) for training and 20% (195 member data set) for testing. Table 5 summarizes the available data used to develop the multiple linear regression (MLR), GEP and ANN models. The parameters in the table include the abutment length (L), flow depth (y), mean flow velocity (U), critical velocity (U_c), mean diameter of the sediment (d_{50}), abutment length ratio (L/y), velocity ratio (U/U_c) and time ratio (t/t_e).

Two types of FFBP models, namely single and double hidden layer systems, were developed to determine the best network for the reliable prediction of scour depth. Based on trials and error, the FFBP network with 4000 epochs and the RBF network

Table 3 Summary of main characteristics of data sets

Researcher(s)	Number of data	L (cm)	y (cm)	d_{50} (mm)	σ_g	U_c (cm/s)	U (cm/s)	L/y	U/U_c	t/t_e	t_e (min)	ds(cm)
A-1 (present study)	199	4	11.1	0.6	1.14	28.75	27.6	0.36	0.96	0∼1	3052	6.7
A-2 (present Study)	188	5.5	11	0.6	1.14	28.75	28.6	0.5	0.96	0∼1	4004	9.5
A-3 (present study)	305	7	9.7	0.6	1.14	28.1	26.7	0.72	0.95	0∼1	5080	11.8
Dey and Barbuhuiya (2005)	111	6∼10	20	0.26∼3.1	1.17∼1.38	28∼ 106	26.0∼67.3	0.3∼0.5	0.63∼0.93	0∼1	1400∼ 2213	12.7∼25.3
Ballio and Orsi (2001)	192	5∼10	9.2∼18.3	5	1.3	77.0∼89.0	77.0∼89.0	0.27∼1.08	∼1	0∼1	16,000∼31,667	11.8∼33.8
Total dataset	995	4∼10	9.2∼20	0.26∼5	1.14∼1.38	28∼106	26.0∼89.0	0.27∼1.08	0.63∼1	0∼1	1400∼31,667	6.7∼33.8

Table 4 Statistical properties for collected data sets

Test data	Number of data	Number of training data	Training			Number of testing data	Testing		
			R^2	RMSE	MAE		R^2	RMSE	*MAE*
All data set	995	800	0.984	0.026	0.0191	195	0.984	0.0273	0.0203
All data set without A-1	796	637	0.980	0.0303	0.022	159	0.980	0.0336	0.0224
All dataset without A-2	807	646	0.983	0.0281	0.0194	161	0.984	0.0273	0.0189
All data set without A-3	690	552	0.987	0.0247	0.0197	138	0.986	0.0265	0.0204
All data set without Dey and Barbuhuiya (2005)	884	707	0.987	0.023	0.0159	177	0.986	0.0235	0.0172
All d data set without Ballio and Orsi (2001)	803	642	0.981	0.0249	0.0167	161	0.988	0.0187	0.0136

Table 5 Range of data for training and testing

	Training		Testing	
Parameter	Min	Max	Min	Max
L (cm)	4.0010.00		4.0010.00	
Y (cm)	9.2020.00		9.2020.00	
U (m/s)	0.260.89		0.260.89	
U_c (m/s)	0.281.06		0.281.06	
d_{50} (mm)	0.26	5.00	0.26	5.00
L/y	0.271.08		0.271.08	
U/U_c	0.631.00		0.631.00	
t/t_e	0.001.00		0.001.00	

with spread constant of 0.7 gave better results compared with the others, and therefore these criteria were selected for the networks.

Since the number of neurons in the hidden layer was unknown, to avoid over-fitting (low training error but high test error), all networks were developed with different numbers of neurons in the hidden layer (Shin and Park 2010). Figure 10 demonstrates the variation of networks in terms of MAE. By increasing the number of neurons, the MAE decreased dramatically in the networks especially for the FFBP method. For the two-layer FFBP when the number of neurons was more than 10, an over fitting of the network was observed. Table 6 shows the performance of the FFBP and RBF networks with different neurons in the hidden layer. The $R^2$and RMSE obtained from the testing data illustrated that the optimum numbers of neurons in the hidden layer for the one-hidden-layer, two-hidden-layer and RBF networks were 14, 8 and 50, respectively. These values were highlighted in bold in Table 6. Analysis of the results indicated that the two-hidden-layer FFBP with eight neurons in each layer ($R^2 = 0.997$, RMSE = 0.0113 and MAE = 0.00714) produced a reliable prediction compared to the one-hidden-layer FFBP with 14 neurons ($R^2 = 0.995$, RMSE = 0.0145 and MAE = 0.0091). Besides, the prediction of FFBP-ANNs with two-hidden-layers and eight neurons in each hidden layer was much better than those obtained by the RBF with 50 neurons in the hidden layer ($R^2 = 0.952$, RMSE = 0.0466 and MAE = 0.0318).

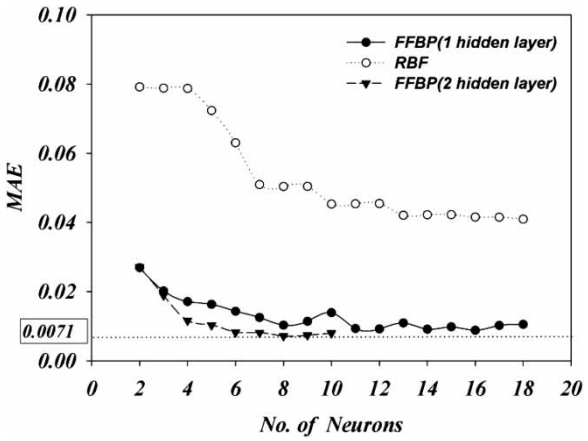

Figure 10 Variation of MAE error in testing data for FFBP and RBF networks.

9 Development of the MLR model

A new regression equation was developed to predict the scour depth based on the three parameters in Eq. 4. The least-squares fit to these observations yielded the expression:

$$\frac{d_s}{d_{se}} = \exp\left[-0.10\left(\frac{U}{U_c}\right)^{-0.267}\left(\frac{y}{L}\right)^{0.314}\left|\mathrm{Ln}\left(\frac{t}{t_e}\right)\right|^{1.13}\right]. \quad (13)$$

Figure 11 shows a comparison between the observed and predicted data using the regression analysis. Equation 13 predicted the scour depth with high accuracy ($R^2 = 0.958$, RMSE = 0.059 and MAE = 0.041) as compared with the existing empirical equations (Table 7).

10 GEP model

GEP is a genetic learning algorithm, which has inherited the advantages of traditional genetic algorithms (GA) and GP. The genome is encoded as linear chromosomes of fixed length expressed as phenotypes in the form of expression trees via GEP. The chromosomes consisted of multiple genes, and each gene encoded a smaller sub-programme. Although the three algorithms of GA, GP and GEP use a population of individuals, the fundamental difference between the algorithms resides in the nature of the individuals. For GEP, the individuals are non-linear entities with different sizes and shapes, and these complex entities are encoded as simple strings of fixed length (chromosomes).

The chromosomes of each individual in the population are generated randomly, and then each individual chromosome is evaluated based on a fitness function, and chosen to reproduce in next generation with modification carried out by the genetic operators. Mutation, as a chromosome modification, is found to be the most effective genetic operator. The same process

Table 6 Neural network results based on statistical measures

Network	No. of neurons		Training			Testing		
	First layer	Second layer	R^2	RMSE	MAE	R^2e	RMSE	MAE
One hidden–layer	11	–	0.996	0.0129	0.0082	0.995	0.0156	0.0093
	12	–	0.996	0.0132	0.0081	0.994	0.0161	0.0092
	13	–	0.996	0.0131	0.0087	0.992	0.0184	0.0109
	14	**–**	**0.996**	**0.0124**	**0.0083**	**0.995**	**0.0145**	**0.0091**
	15	–	0.997	0.0116	0.0075	0.994	0.0159	0.0098
Two hidden-layer	6	6	0.997	0.0097	0.00635	0.995	0.0143	0.0082
	7	7	0.998	0.0077	0.0053	0.995	0.0151	0.0081
	8	**8**	**0.998**	**0.0079**	**0.0051**	**0.997**	**0.0113**	**0.00714**
	9	9	0.999	0.0058	0.004	0.993	0.0184	0.00737
	10	10	0.999	0.00545	0.0036	0.993	0.0178	0.00795
	11	11	0.999	0.00544	0.0035	0.917	0.0614	0.0125
RBF (spread constant = 0.7)	12	–	0.893	0.0679	0.0444	0.891	0.0702	0.0454
	13	–	0.902	0.0652	0.0422	0.899	0.0675	0.0421
	14	–	0.908	0.0631	0.0419	0.905	0.0657	0.0422
	15	–	0.907	0.0634	0.042	0.904	0.0659	0.0423
	20	–	0.928	0.0558	0.0381	0.921	0.06	0.0399
	30	–	0.939	0.0514	0.036	0.939	0.0527	0.0365
	40	–	0.945	0.0489	0.034	0.946	0.0495	0.0337
	50	**–**	**0.95**	**0.0467**	**0.0319**	**0.952**	**0.0466**	**0.0318**

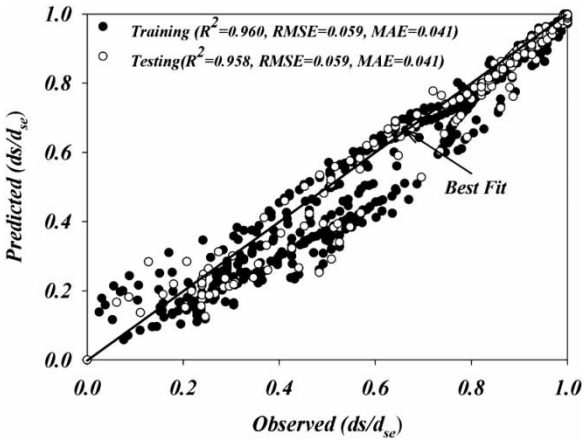

Figure 11 Comparison between observed and predicted data using MLR.

occurred for new individuals and this trend was repeated until the required accuracy was achieved for a predefined number of generations (Ferreira 2001a, 2001b). To modify the chromosomes, several genetic operations were used, mutation, inversion, insertion sequence transposition, root insertion sequence transposition and gene cross-over (Ferreira 2006).

11 Development of GEP for temporal scour depth

To evaluate the scour depth, the GEP model was developed using the same data set used for the ANNs.

The first step is the selection of the number of chromosomes and genes for the initial population of individuals. Ferreira (2001b) showed that a population of 30–100 chromosomes might provide a good result. In this study, a population size of

Table 7 Performance indices of various approaches to predict the time-dependence of scour depth

Z	Training			Testing		
	R^2	RMSE	MAE	R^2	RMSE	MAE
FFBP (two-hidden-layer)	0.998	0.0079	0.0051	0.997	0.0113	0.0071
GEP	0.962	0.060	0.037	0.959	0.068	0.044
Present regression (Eq. 13)	0.960	0.059	0.041	0.958	0.059	0.041
Coleman et al. (2003)	0.942	0.076	0.059	0.936	0.078	0.062
Cardoso and Bettess (1999)	0.943	0.104	0.087	0.932	0.100	0.081
Yanmaz and Kose (2007)	0.809	0.217	0.191	0.823	0.205	0.176
Ballio and Orsi (2001)	0.888	0.247	0.224	0.903	0.244	0.220
Oliveto and Hager (2002)	0.634	0.460	0.400	0.594	0.503	0.436

Table 8 Parameters of the optimized GEP model

Description of parameter	Setting of parameter
Function set	(+, −, *, /, sqrt, power)
Population size	50
Head length	7
Number of genes	3
Mutation rate (%)	30
Linking function	Addition
Inversion rate (%)	30
One-point recombination rate (%)	30
two-point recombination rate (%)	30
Gene recombination rate	0.1
Gene transportation rate	0.1

50 chromosomes was therefore selected as the optimal size and was subsequently used in modelling.

Second, the fitness function of individuals was computed using the MSE as the fitness function

$$f_i = 1000\frac{1}{1+E_i} \quad \text{for} \quad E_i = P_{ij} - O_j, \tag{14}$$

where P_{ij} is the predicted value by individual chromosome i for fitness case j and O_j is the observed value for fitness case j. The perfect solution with no error ($E_{ij} = 0$) occurs when $P_{ij} = O_{ij}$.

In third step, the set of functions and terminals were chosen for each gene to create the chromosomes. In this work, four basic arithmetic operators (+, −, * and /) and two basic mathematical functions (power and sqrt) were used as functions,

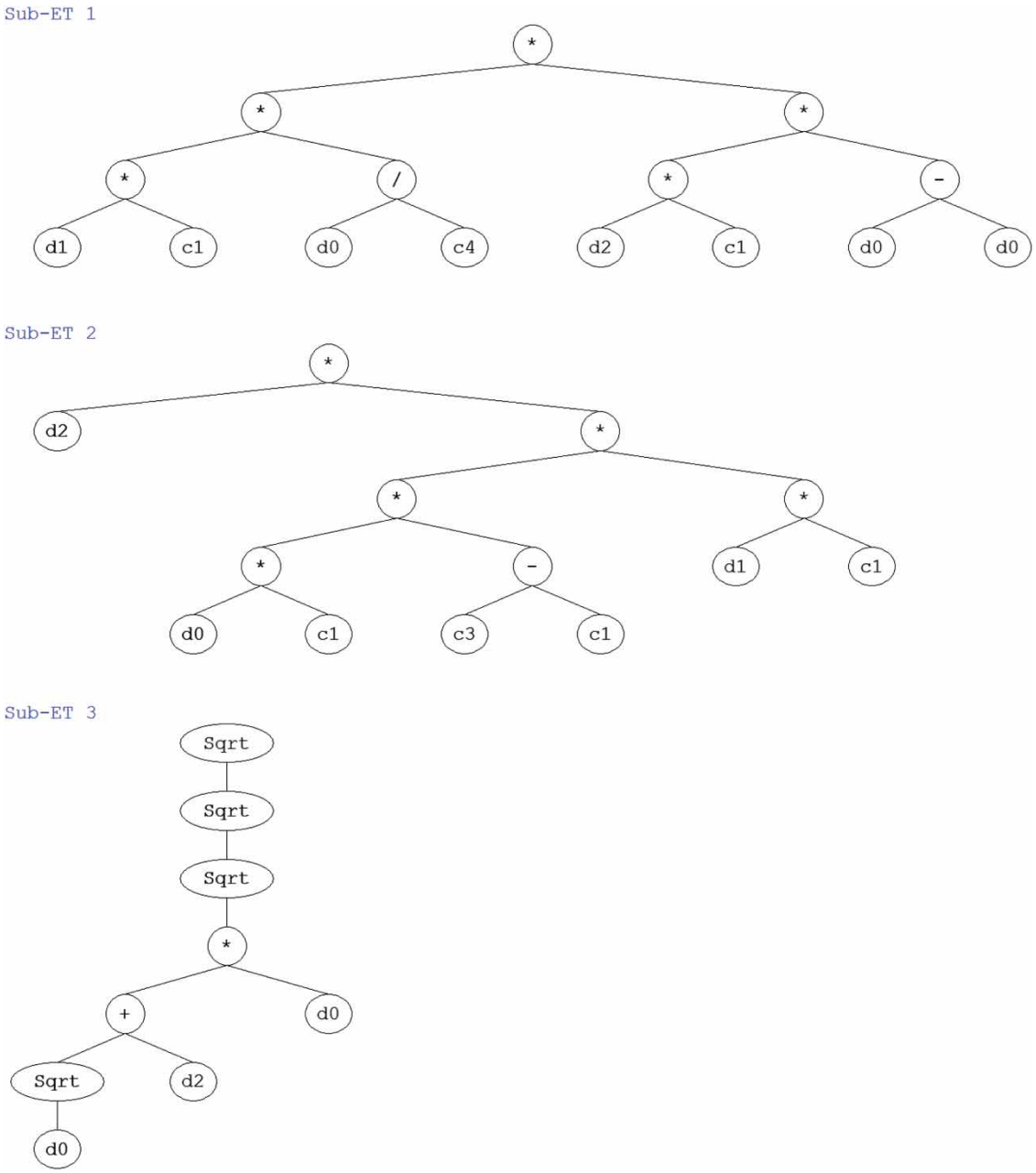

Figure 12 Expression trees for the GEP formulation.

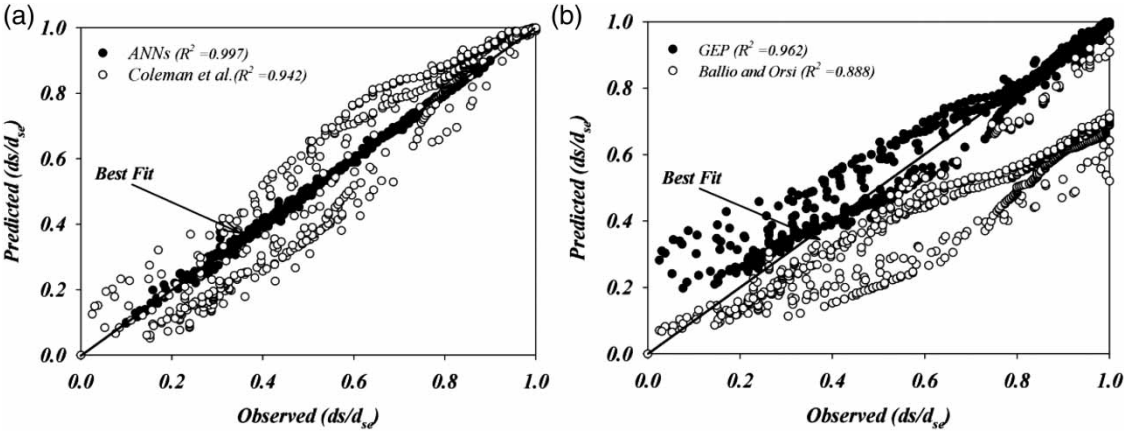

Figure 13 Comparison between conventional equation and (a) ANN modelling and (b) GEP modelling.

while the set of terminals included the three independent variable in Eq. 4, i.e. $T = \{t/t_e, U/U_c, y/L\}$.

The selection of chromosome architecture (number of genes and the length of the head and tail) is the fourth step of GEP modelling. The head and tail are two parts of genes, each with different functions and properties. The head is utilized mostly to encode the variables and functions chosen to solve the problem, whereas the tail, while also used to encode the variables, provides essentially a reservoir of terminals to ensure that all programmes are error-free. Increasing in the number of genes from one to three significantly increased the success rate (Ferreira, 2001b), and the best result was obtained with three genes per chromosome and a length head equal to 7.

The fifth step is to decide the linking function. The chromosomes of GEP are generally composed of more than one gene.

Table 9 Sensitive analysis results for non-dimensional parameters

		Training			Testing		
Model	No. of neurons	R^2e	RMSE	MAE	R^2	RMSE	MAE
Without U/Uc							
Epoch = 4000	10	0.989	0.0208	0.0126	0.987	0.0243	0.0142
	11	0.99	0.0198	0.0116	0.986	0.0246	0.0136
	12	0.993	0.0171	0.0106	0.989	0.0223	0.0134
	13	0.992	0.0186	0.0105	0.989	0.0217	0.0121
	14	0.993	0.0169	0.0096	**0.990**	**0.0212**	**0.0118**
	15	0.992	0.0184	0.01	0.989	0.0226	0.0117
	16	0.992	0.0189	0.0105	0.988	0.0229	0.0131
Without *L/y*							
Epochs = 4000	10	0.965	0.0397	0.0286	0.974	0.0336	0.0231
	11	0.99	0.0207	0.014	0.981	0.0289	0.017
	12	0.989	0.0219	0.0145	0.986	0.0253	0.0175
	13	0.991	0.0192	0.0131	0.986	0.0246	0.0164
	14	0.992	0.0184	0.012	**0.986**	**0.0244**	**0.0149**
	15	0.992	0.0185	0.0124	0.981	0.0293	0.0164
	16	0.991	0.0198	0.013	0.985	0.0261	0.017
Without t/t_e							
Epochs = 4000	10	0.382	0.163	0.125	0.194	0.192	0.145
	11	0.381	0.163	0.125	0.194	0.192	0.145
	12	0.381	0.163	0.125	0.194	0.192	0.145
	13	0.381	0.163	0.125	0.194	0.192	0.145
	14	0.381	0.163	0.125	0.194	0.192	0.145
	15	0.381	0.163	0.125	0.194	0.192	0.145
	16	0.381	0.163	0.125	0.194	0.192	0.145

Each gene codes for a sub-programme (sub-ET in Figure 12) or sub-expression tree. Then the sub-programme can interact with one another in different ways, forming a more complex programme. In the GEP model, the sub-expression three must be linked through the linking function. Both the addition and multiplication operators were tested in the model and it was found that the addition function provided a better fitness value.

In the last step, the genetic operators, such as mutation, inversion, transpositions, recombination or cross-over, were used to select the variation of the genetic material. A summary of the parameters is shown in Table 8. The simplified analytic form of the proposed GEP model may be expressed as

$$\frac{d_s}{d_{se}} = \left[\left(\sqrt{\frac{t}{t_e}} + \frac{L}{y}\right)\frac{t}{t_e}\right]^{0.125} - 0.081\left(\frac{t}{t_e}\right)\left(\frac{U}{U_c}\right)\left(\frac{L}{y}\right). \quad (15)$$

The corresponding expression trees are shown in Figure 12.

12 Result and discussion

The performance of the GEP model was compared with the MLR and ANN models. Table 7 indicates that although the equation of Coleman et al. (2003) has acceptable result ($R^2 = 0.936$ and MAE = 0.062) as compared with other conventional equation, the presented regression model (Eq.13) predicts the scour depth with high accuracy ($R^2 = 0.958$ and MAE = 0.041). A comparison between the neural network and conventional equations is shown in Figure 13(a). The results (Table 7) show that the FFBP provided a better result ($R^2 = 0.997$, RMSE = 0.0113 and MAE = 0.0071) than the GEP model ($R^2 = 0.959$, RMSE = 0.068 and MAE = 0.044). Comparisons of performance from error statistics (Table 7) and scatter plots (Figure 13(b)) illustrated that the GEP model provided a better prediction than previous and presented regression models.

13 Sensitivity analysis

To determine the relative importance of input variables on the time-dependent scour depth, a sensitivity analysis was carried out using the ANN models. The sensitivity analysis was performed with a one-hidden-layer FFBP network with different neurons and epoch equal to 4000. The results of the sensitivity analysis for the three independent variables are summarized in Table 9 by removing a parameter in each case. The parameters were compared based on the correlation coefficient, RMSE and MAE and optimum number of neurons was highlighted in bold. It is apparent from this table and Figure 14 that the three independent parameters have a non-negligible influence on d_s/d_{se} and that the time ratio (t/t_e) is a significant parameter in determining the time-dependent scour depth, while velocity ratio (U/U_c) has the least influence on d_s/d_{se}. The effects of the non-dimensional variables on the time-dependent scour depth can be ranked in the order of $t/t_e > L/y > U/U_c$ (Figure 14). A similar trend was reported for time-dependent scour depth around pile bridge (Bateni et al. 2007).

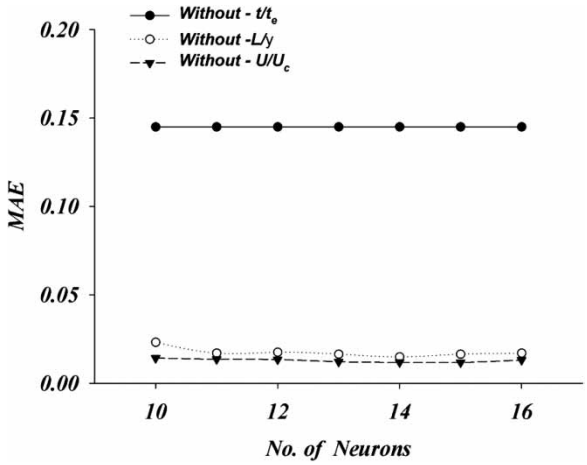

Figure 14 Sensitivity analysis in terms of number of neurons and MAE.

14 Conclusions

Time is a significant parameter for prediction of scour depth around the abutment. The experiments were conducted for a short abutment ($L/y \leq 1$) in threshold conditions with uniform sediment and deep water. Results indicated that the dimension of the scour hole was limited to $3L$ and $5L$ upstream and downstream of the abutment, respectively, in the X-direction. The dimension of the scour hole in the Y-direction (perpendicular to flow direction) was limited to $4L$. The upstream slope was also 30–60% greater than the downstream slope. The flow deposited the sediment at $X/L = 5$ and deposition continued to $X/L = 16$ downstream of the abutment.

Three methods MLR, ANNs and the GEP were employed to predict the time variation of scour, the presented MLR model provided better results ($R^2 = 0.958$, RMSE = 0.059 and MAE = 0.041) compared with previous equations (Table 7). Two ANN models, namely FFBP and RBF models were developed to predict the time variation of scour depth. To select the optimum ANN, both FFBP and RBF with different neurons in the hidden layer were tested. A two-hidden-layer FFBP with eight neurons within each layer was selected as the best ANN ($R^2 = 0.997$, RMSE = 0.0113 and MAE = 0.00714). The performance of the optimal explicit equation developed from GEP ($R^2 = 0.959$ and MAE = 0.044) was found better than the conventional equations and comparable with the ANN models. The sensitivity analysis showed that the effects of the non-dimensional variables on temporal scour depth can be ranked in the order of $t/t_e > L/y > U/U_c$. The presented GEP and regression models can be used to predict time variation of scour depth at short abutment in rivers with high accuracy in comparison with previous equations.

Notation

The following symbols are used in this paper:

B	abutment width
d_s	scour depth at time t
d_{se}	equilibrium scour depth
d_{50}	median size of the bed material
F_d	$U/\sqrt{\Delta g d_{50}}$ (particles Froude number)
I	flow intensity
g	gravity acceleration
I	flow intensity
K_G	coefficient of channel cross-section geometry
K_θ	coefficients of abutment alignment
K_s	coefficients of abutment shape
L	abutment length
n	number of data
Re	UL/ν (abutment Reynolds number)
t	time of scouring
t_e	equilibrium time of scouring
T^*	time when $d_s = 0.632 d_{se}$
U	mean flow velocity
U_c	critical velocity for the beginning of motion of bed material
X, Y	coordinate system
y	approach flow depth
b_i	bias
E_i	error value
O_i	observed value
O_j	observed value for fitness case j
$\bar{O}_i$	average of observed value
P_{ij}	predicted value by individual chromosome i
t_i	predicted value
w_i	ith weight of network
X_n	normalized value of X
x_i	neuron value
$\varphi(x)$	softmax transfer function
ρ	fluid density
ρ_s	sediment density
ν	fluid kinematic viscosity
σ_g	geometric standard deviation
$\Delta = (\rho_s - \rho)/\rho$ (relative density)	
μ_j	centre of RBF
σ_j	radius of RBF

References

Azamathulla, H.M., 2012. Gene-expression programming to predict scour at a bridge abutment. *Journal of Hydroinformatics*, 14 (2), 324–331.

Azamathulla, H., Ab. Ghani, A., Zakaria, N.A., and Guven, A. (2010). Genetic Programming to Predict Bridge Pier Scour. *J. Hydraul. Eng.*, 136 (3), 165–169.

Ballio, F. and Orsi, E., 2001. Time evolution of scour around bridge abutments. *Water Engineering Research*, 2 (4), 243–259.

Bateni, S.M. and Jeng, D.S., 2007. Estimation of pile group scour using adaptive neuro-fuzzy approach. *Ocean Engineering*, 34 (8–9), 1344–1354.

Bateni, S.M., Jeng, D.S., and Melville, B.W., 2007. Bayesian neural networks for prediction of equilibrium and time-dependent scour depth around bridge piers. *Advances in Engineering Software*, 38 (2), 102–111.

Begum, S.A., Fujail, A.K.M., and Barbhuiya, A.K., 2011. Radial basis function to predict scour depth around bridge abutment. *In 2nd national conference on emerging trends and applications in computer science (NCETACS).* Shillong, Meghalaya, India. 76–82.

Begum, S.A., Fujail, A.K.M., and Barbhuiya, A.K., 2012. Artificial neural network to predict equilibrium local scour depth around semicircular bridge abutments. *6thSASTech 2012*, 24–25 March 2012, Malaysia, Kuala Lumpur. Organized by Khavaran Institute of Higher Education.

Brandimarte, L., Paron, P., and Di baldassarre, G., 2012. Bridge pier scour: a review of processes, measurements and estimates. *Environmental Engineering and Management Journal*, 11 (5), 975–989.

Cardoso, A.H. and Bettess, R., 1999. Effects of time and channel geometry on scour at bridge abutments. *Journal of Hydraulic Engineering*, 125 (4), 388–399.

Coleman, S.E., Lauchlan, C.S., and Melville, B.W., 2003. Clear-water scour development at bridge abutments. *Journal of Hydraulic Research*, 41 (5), 521–531.

Dey, S. and Barbhuiya, A.K., 2005. Time variation of scour at abutments. *Journal of Hydraulic Engineering*, 131 (1), 11–23.

Ferreira, C., 2001a. Gene expression programming in problem solving (invited tutorial). *Proceedings of 6th online world conference on soft computing in industrial applications*. Berlin: Springer.

Ferreira, C., 2001b. Gene expression programming: a new adaptive algorithm for solving problems. *Complex Systems*, 13 (2), 87–129.

Ferreira, C., 2006. *Gene-expression programming; mathematical modeling by an artificial intelligence*. Berlin: Springer.

Khan, M., Azamathullah, H.Md., Tufail, M. and Ab. Ghani, A. (2012). Bridge Pier Scour Prediction by Gene-expression Programming. *Proceedings of ICE – Water Management*, 165 (9) 481–493.

Kwan, T.F. and Melville, B.W., 1994. Local scour and flow measurements at bridge piers. *Journal of Hydraulic Research*, 32 (5), 661–674.

Lim, S.-Y., 1997. Equilibrium clear-water scour around an abutment. *Journal of Hydraulic Engineering*, 123 (3), 237–243.

Melville, B.W., 1992. Local scour at bridge abutments. *Journal of Hydraulic Engineering-Asce*, 118 (4), 615–631.

Melville, B.W. and Coleman, S.E., 2000. *Bridge scour*. Colorado, USA: Water Resources Publications, 550.

Muzzammil, M., 2010. ANFIS approach to the scour depth prediction at a bridge abutment. *Journal of Hydroinformatics*, 12 (4), 475–485.

Muzzammil, M., 2011. ANFIS-base approach to scour depth prediction at abutment in armored bed. *Journal of Hydroinformatics*, 13 (4), 669–713.

Oliveto, G. and Hager, W.H., 2002. Temporal evolution of clear-water pier and abutment scour. *Journal of Hydraulic Engineering*, 128 (9), 811–820.

Sarlak, N. and Tigrek, S., 2011. Analysis of experimental data sets for local scour depth around bridge abutments using artificial neural networks. *Water Sa*, 37 (4), 595–602.

Shin, J.H. and Park, H.I., 2010. Neural network formula for local scour at piers using field data. *Journal of Marine Georesources & Geotechnology*, 28 (1), 37–48.

Simarro, G., Teixeira, L., and Cardoso, A.H., 2007. Flow intensity parameter in pier scour experiments. *Journal of Hydraulic Engineering*, 133 (1), 1261–1264.

Sturm, T.W. and Janjua, N.S., 1994. Clear-water scour around abutments in floodplains. *Journal of Hydraulic Engineering*, 120 (8), 956–972.

Toth, E. and Brandimarte, L., 2011. Prediction of local scour depth at bridge piers under clear-water and live-bed conditions: comparison of literature formulae and artificial neural networks. *Journal of Hydroinformatics*, 13 (4), 812–824.

Yanmaz, A.M. and Kose, O., 2007. Time-wise variation of scouring at bridge abutments. *Sadhana-Academy Proceedings in Engineering Sciences*, 32 (3), 199–213.